Coherent states of the driven Rydberg atom: Quantum-classical correspondence of periodically driven systems

Luz V. Vela-Arevalo* and Ronald F. Fox†
Center for Nonlinear Science, School of Physics, Georgia Institute of Technology, Atlanta, Georgia 30332-0430, USA
(Received 14 January 2005; published 9 June 2005)

A methodology to calculate generalized coherent states for a periodically driven system is presented. We study wave packets constructed as a linear combination of suitable Floquet states of the three-dimensional Rydberg atom in a microwave field. The driven coherent states show classical space localization, spreading, and revivals and remain localized along the classical trajectory. The microwave strength and frequency have a great effect in the localization of Floquet states, since quasienergy avoided crossings produce delocalization of the Floquet states, showing that tuning of the parameters is very important. Using wavelet-based time-frequency analysis, the classical phase-space structure is determined, which allows us to show that the driven coherent state is located in a large regular region in which the z coordinate is in resonance with the external field. The expectation values of the wave packet show that the driven coherent state evolves along the classical trajectory.

DOI: 10.1103/PhysRevA.71.063403 PACS number(s): 32.80.Wr, 03.65.−w, 05.45.−a, 95.10.Fh

I. INTRODUCTION

Construction of coherent states provides the basic understanding of quantum dynamics in the classical limit and yields some insight into control of quantum systems. In this work, we provide a methodology to construct coherent states for a periodically driven Hamiltonian: the Rydberg atom in a microwave field. We calculate a Gaussian-generalized coherent state for the Floquet Hamiltonian in the extended phase space. The wave packet so constructed shows classical space localization, spreading, and revivals along the classical trajectory, as an evidence of quantum-classical correspondence.

Coherent states are characterized by their localized electronic density in both configuration and momentum space. As proposed by Schrödinger in 1926 [1], they are states of minimum uncertainty that peak along the classical orbit. The study of coherent states was initially focused on the simple harmonic oscillator for which the coherent states are eigenstates of the annihilation operator. These coherent states form a nonorthogonal basis, admit a resolution of the identity operator, and evolve into coherent states. Glauber [2] discovered that the coherent states of the harmonic oscillator can be obtained with a displacement operator acting on a reference state. This last property was used by Zhang *et al.* [3] to define generalized coherent states as (a) states obtained with a displacement operator acting on a reference state, (b) that are parametrized continuously, (c) that are temporally stable (i.e., they evolve into coherent states), and (d) that provide the resolution of the identity operator.

Many constructions of coherent states for the hydrogen atom have been proposed; for instance, circular coherent states were first proposed by Brown [4] and elliptic coherent states by Mostowski [5], as an application of coherent states for arbitrary dynamical groups proposed by Perelomov [6] and Barut [7]. Yeazell and Stroud [8] attempted to make Rydberg atom wave packets that are localized in the angle variables; they observe precession of the ellipse caused by a perturbation to the Hamiltonian caused by the quantum defect of alkali-metal atoms. However, those and later constructions of coherent states do not satisfy the resolution of the identity operator, nor are they temporally stable. Klauder [9] constructed generalized coherent states for the hydrogen atom, which are obtained with a displacement operator and provide a resolution of the identity operator. However, Klauder's generalized coherent states fail to be localized in configuration space. Fox [10] proposed Gaussian generalized coherent states for hydrogen which satisfy the same properties as Klauder's, but that are also localized.

Localized wave packets of hydrogen were first observed experimentally when the atom was exposed to a short intense laser pulse, producing the excitation of a broad range of energy levels, in an experiment by ten Wolde *et al.* [11]. These wave packets were the realization of analytical radial coherent states proposed by Parker and Stroud [12] for the one-dimensional hydrogen Hamiltonian, using the rotating-wave approximation, in an external field of a picosecond laser pulse. They also discussed the decay and revival of the wave packet. A semiclassical formalism of the generation of wave packets with short pulses was proposed by Alber *et al.* [13]. Gay *et al.* [14] found that elliptic coherent states can be found for hydrogen in circularly polarized electric and magnetic fields. Circular coherent states were also found for hydrogen driven by circularly polarized electric and magnetic fields, which correspond to localized wave packets around fixed points that are the analog of the Lagrangian fixed points of the restricted three-body problem [15]. In [16], wave packets localized in the radial direction were calculated for hydrogen in a linearly polarized microwave field, which corresponds to a periodically driven Hamiltonian; these wave packets are calculated as Floquet states which are *nondispersive* states. The nondispersive wave packets in a linearly polarized field in the z direction are axially symmetric with

*Electronic address: luzvela@cns.physics.gatech.edu
†Electronic address: ron.fox@physics.gatech.edu

respect to the z axis; hence, they are not localized in the azimuthal φ angle. Particularly, the nondispersive states in [16] were obtained for angular momentum quantum number $m=0$; therefore, those Floquet states are very similar to Floquet states for the one-dimensional model, and they are radially localized, but extend linearly in the z direction, and are axially symmetric. Elliptic coherent states in weak crossed electric and magnetic fields and its classical correspondence were studied by Bellomo *et al.* [17] Nondispersive wave packets obtained semiclassically that are located in the classical resonance islands are described in [18]. More recently, Maeda and Gallagher [19] and Maeda *et al.* [20] observed nondispersive one-dimensional (linear) wave packets for lithium driving the system with a field resonant with a $\Delta n=1$ transition for n around 75. Perhaps similar techniques could be used to test the circular coherent states that we study.

We construct localized wave packets for hydrogen in a linearly polarized microwave field by applying the construction of Gaussian-generalized coherent states [10] to the Floquet Hamiltonian in the extended phase space. The wave packet we propose is formed by Floquet states which are localized both radially and in the polar angle (θ). The Floquet states we use resemble circular hydrogen states, but now they oscillate in the z direction due to the external field. Since circular states in a linearly polarized field are more stable than linear states [21], in the sense that they require larger field strength to ionize, the wave packets have a long lifetime and the coupling with unbound states is negligible for the integration times in this work. Localization in the azimuthal angle (φ) is achieved by the superposition of several Floquet states.

In the construction of driven coherent states, it is important to understand the system's response to the microwave parameters: frequency and strength. The appearance of avoided crossing of the quasienergies as the parameters vary has a dramatic effect on the components of Floquet states [22]. A quasienergy avoided crossing results in a loss of classical space localization. Hence, tuning of the parameters is crucial.

Our driven generalized coherent states provide great insight into the quantum-classical correspondence. The classical system has three degrees of freedom with explicit time dependence (phase space of dimension 7); we propose the use of wavelet time-frequency analysis to unravel the classical phase-space dynamics. This method has been used previously in celestial mechanics [23] and in molecular systems [24]; in this work, however, it is the first time that the method will be used to compare the purely quantum dynamics with the classical one. This method allows us to detect both regular and chaotic regions of the phase space, as well as locking between the internal frequency and the external field. We show that the driven coherent states are classically localized in a wide regular region in which the dynamics of the coordinate parallel to the field is in resonance with the external field. Furthermore, the dynamical evolution of our proposed driven coherent states coincides with the classical trajectory of the electron, evidencing the classical-quantum correspondence of the driven Rydberg electron.

In the next section, we state the Hamiltonian for the hydrogen atom in a linearly polarized microwave field, both in the velocity and length gauges. In Sec. III a quick review of Gaussian-generalized coherent states of unperturbed hydrogen is presented, since this definition will be applied to the Floquet Hamiltonian in the extended phase space. In Sec. IV, we describe the calculation of Floquet states of hydrogen in a microwave field and analyze their classical configuration-space localization as a function of microwave parameters. In Sec. V, we propose a methodology to construct generalized coherent states for the driven system. In Sec. VI, we describe the classical phase-space structure using the wavelet-based frequency analysis method and show that the wave packet obtained in Sec. V travels along the classical orbit, showing quantum-classical correspondence in the system. Conclusions are in Sec. VII.

II. RYDBERG ATOM IN A LINEARLY POLARIZED RADIATION FIELD

The Rydberg Hamiltonian in a microwave field, in atomic units is given by

$$H=\frac{1}{2}[\vec{p}+\vec{A}(t)]^2-\frac{1}{r}. \tag{1}$$

The radiation field $\vec{A}$ is linearly polarized in the direction of the z axis, and it is represented by $\vec{A}(t)=\hat{k}(\lambda/\omega)\sin(\omega t)$, where λ is the strength of the microwave and ω its frequency. The Hamiltonian (1) is in the so-called velocity gauge. The Goeppert-Mayer gauge transformation [22] transforms the Hamiltonian in the so-called length gauge, given by the dipole Hamiltonian

$$H=H_0-\lambda\cos(\omega t)z, \tag{2}$$

where H_0 is the unperturbed hydrogen-atom Hamiltonian,

$$H_0=\frac{p^2}{2}-\frac{1}{r}. \tag{3}$$

The bound eigenstates and eigenenergies of Eq. (3) are denoted by the equation

$$H_0|\phi_k\rangle=e_k|\phi_k\rangle. \tag{4}$$

The indices k correspond to the usual quantum numbers n,l,m, with n the principal quantum number; $l=0,\ldots,n-1$ and $m=-l,\ldots,l$. The eigenenergies are determined by n as $e_k=e_n=-1/(2n^2)$.

The classical equations of motion for Hamiltonian (2) are invariant under the following transformation:

$$h'=hn_0^2,\quad \vec{r}'=\vec{r}/n_0^2,\quad \vec{p}'=\vec{p}n_0,$$

$$t'=t/n_0^3,\quad \omega'=\omega n_0^3,\quad \lambda'=\lambda n_0^4, \tag{5}$$

where $h=H(\vec{r},\vec{p},t)$ and n_0 is a positive constant. For our purpose, the dynamics will be rescaled by the principal quantum number n_0 representing the center of the wave packet. It is common to express the microwave parameters rescaled according to the previous transformation, as λ'/n_0^4 and ω'/n_0^3.

The time-dependent solution $|\psi(t)\rangle$ of the Schrödinger equation for the Rydberg Hamiltonian (1) can be expanded using the Goeppert-Mayer gauge transformation [22]

$$|\psi(t)\rangle = \exp\left(-\frac{i\lambda}{\omega} z \sin(\omega t)\right) \sum_k a_k(t)|\phi_k\rangle, \tag{6}$$

where $|\phi_k\rangle$ are the unperturbed states of hydrogen (4). The coefficients $a_k(t)$ must satisfy the auxiliary equations [22]

$$\frac{da_k}{dt} = -ie_k a_k + i\lambda \cos(\omega t) \sum_j \langle \phi_k|z|\phi_j\rangle a_j. \tag{7}$$

The auxiliary equations provide the time-dependent solution for the length-gauge Hamiltonian (2):

$$|\tilde{\psi}(t)\rangle = \sum_k a_k(t)|\phi_k\rangle. \tag{8}$$

III. GAUSSIAN-GENERALIZED COHERENT STATES OF UNPERTURBED HYDROGEN

The Gaussian-generalized coherent states were proposed by Fox [10] to construct states that are localized in configuration space and form a nonorthogonal basis satisfying the resolution of the identity operator.

The Gaussian-generalized coherent states [10] for a nondegenerate Hamiltonian are given by

$$|G, n_0, \varepsilon_0\rangle = \sum_{n=0}^{\infty} \frac{\exp\left[-\frac{1}{4}\frac{(n-n_0)^2}{\sigma^2}\right]}{[N(n_0)]^{1/2}} e^{ie_n\varepsilon_0}|n\rangle, \tag{9}$$

where $e_1 < e_2 < \cdots$ are the eigenenergies, $|n\rangle$ are the eigenstates, and

$$N(n_0) = \sum_{n=0}^{\infty} \exp\left[-\frac{(n-n_0)^2}{2\sigma^2}\right]. \tag{10}$$

The definition of $N(n_0)$ guarantees normalization:

$$\langle G, n_0, \varepsilon_0|G, n_0, \varepsilon_0\rangle = 1.$$

The previous definition is slightly modified for the case of degenerate Hamiltonians [25].

For unperturbed hydrogen (3), the eigenstates with $l=m=n-1$ are called *circular states* since their electronic density $|\phi_{n,l,m}(x,y,z)|^2$ is localized in a circular band close to the (x,y) plane and remains around the circular orbit for the Kepler problem. Figure 1 shows the circular state $|\phi_{35,34,34}\rangle$. Circular states are localized both in r and in the angle θ; however, localization in the azimuthal angle φ requires superposition of states with different m quantum numbers.

The circular Gaussian-generalized coherent states [10] are obtained by considering only circular states in expression (9). A wave packet so constructed is shown in Fig. 2. The circular Gaussian coherent states evolve in time along the classical Kepler orbit with the classical period given by $\tau = 2\pi n_0^3$ [10]. Since these coherent states are constructed as the superposition of unperturbed states with different

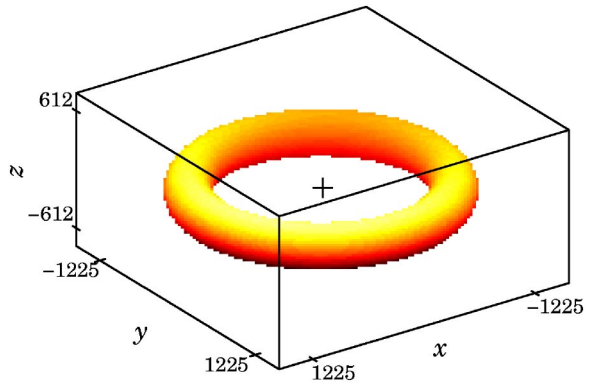

FIG. 1. (Color online) Electronic distribution of a circular state of hydrogen with $n=35$, $l=m=n-1$ in Cartesian configuration space.

eigenenergies, its time evolution will produce delocalization in the φ angle [10]. The delocalization is illustrated in Fig. 2, where the electronic distribution of a circular Gaussian coherent state with $n_0=35$, $\varepsilon_0=0$, and $\sigma=1$ is plotted for different time points normalized by the Kepler period τ. The state follows the classical orbit until it collapses at $t=3\tau$. A half revival occurs at $t=6\tau$ and a full revival is produced at $t=12\tau$.

The Kepler period coincides with the recurrence time of the wave packet defined by Eq. (9). The recurrence time as well as the collapse and revival times for a wave packet have been calculated in general [18]:

$$T_{\text{recurrence}} = 2\pi\left(\frac{dE_n}{dn}(n_0)\right)^{-1},$$

$$T_{\text{collapse}} = 2\left((\Delta n)^2 \frac{d^2E_n}{dn^2}(n_0)\right)^{-1},$$

$$T_{\text{revival}} = 2\pi\left(\frac{d^2E_n}{dn^2}(n_0)\right)^{-1}. \tag{11}$$

For the case of the hydrogen atom $T_{recurrence}=\tau=2\pi n_0^3$, $T_{\text{collapse}}=2n_0^4/(3\Delta n^2)$, and $T_{\text{revival}}=2\pi n_0^4/3$. Δn is the number of significant energy levels in the wave packet.

Dependence on n_0, ε_0, σ

The Gaussian-generalized coherent states (9) are defined in terms of three parameters: n_0, the center of the Gaussian distribution; σ, the standard deviation of the Gaussian; and ε_0, initial phase factor of the superposition of states. The motion of the wave packet along the classical orbit is determined by n_0. The radius of the circular orbit is n_0^2, and as was mentioned previously, the Kepler period and collapse and revival times depend only on n_0.

On the other hand, σ and ε_0 determine the initial localization properties of the generalized coherent state and have important effect on the collapse and revival times of the wave packet. ε_0 determines the initial phase distribution of the states forming the wave packet, which is equivalent to s

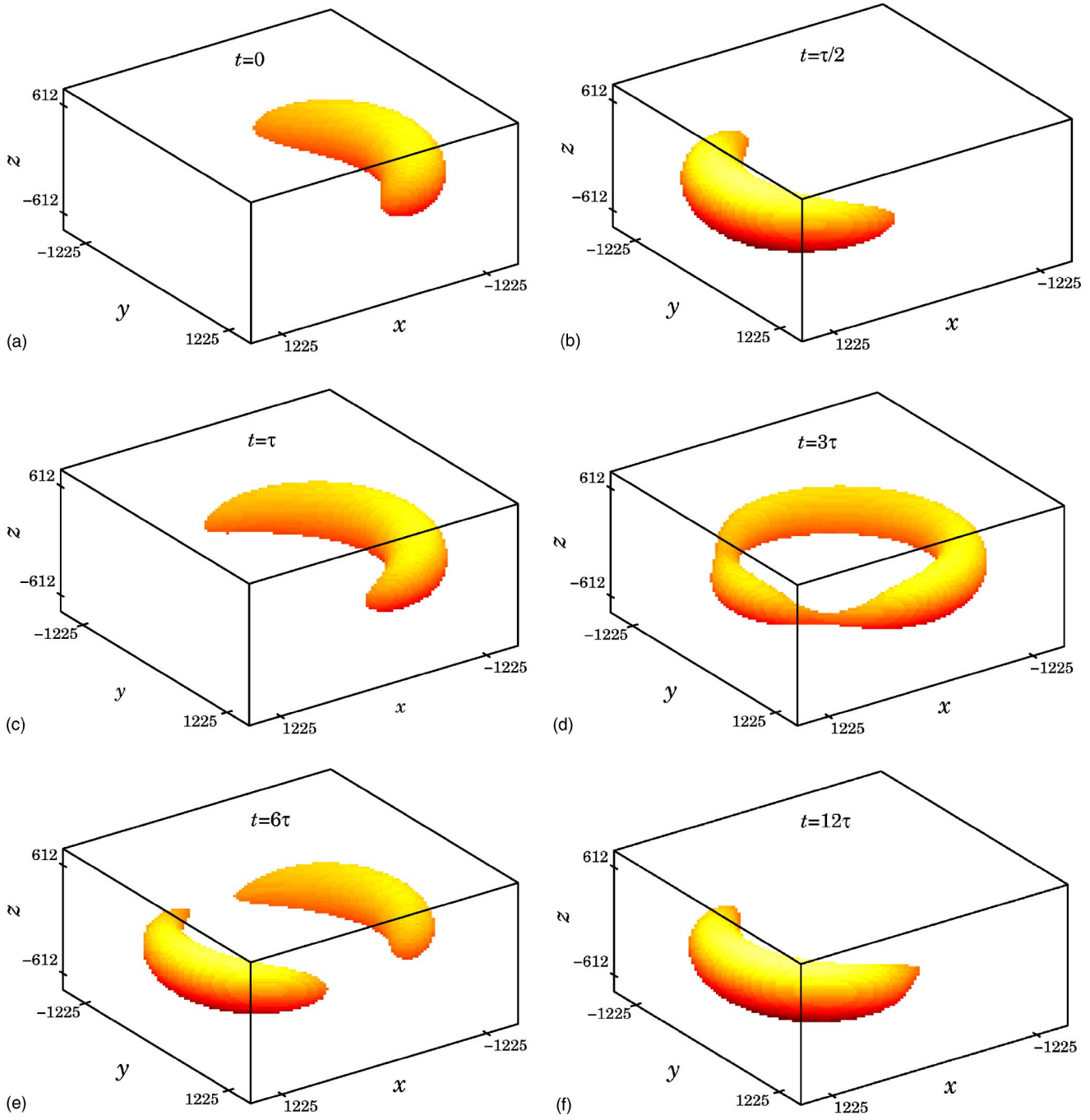

FIG. 2. (Color online) Circular Gaussian-generalized coherent state (9) centered around $n_0=35$ and with standard deviation $\sigma=1$. Delocalization in the azimuthal angle φ occurs in its time evolution. The time points are normalized by the Kepler period $\tau=2\pi n_0^3$. The wave packet follows the Kepler orbit. It collapses at $t=3\tau$, a half revival occurs at 6τ and a first revival at 12τ.

fixing the initial time t for the evolution of the wave packet. For our purposes, we set $\varepsilon_0=0$ and the initial time $t=0$.

The standard deviation σ determines the quantum states that effectively form the coherent state in the sum (9). A very small σ produces a wave packet formed by one single state. A large standard deviation produces a wave packet formed by a Gaussian distribution of many states. For the case of circular states ($l=m=n-1$), coherent states with large σ produce a wave packet that is initially well localized. Small σ, on the other hand, produces wave packets with less superimposed states and therefore initially less localized. However, this has a significant consequence regarding the time evolution of the wave packet. Coherent states with large σ delocalize more quickly due to the fact that more eigenenergies dephase faster, also producing weaker revivals. And coherent states with small σ have longer collapse times and stronger revivals. To illustrate this, we calculate the autocorrelation function for coherent states with different σ. For general wave packets $|G\rangle$, the autocorrelation function [26,27] is defined as

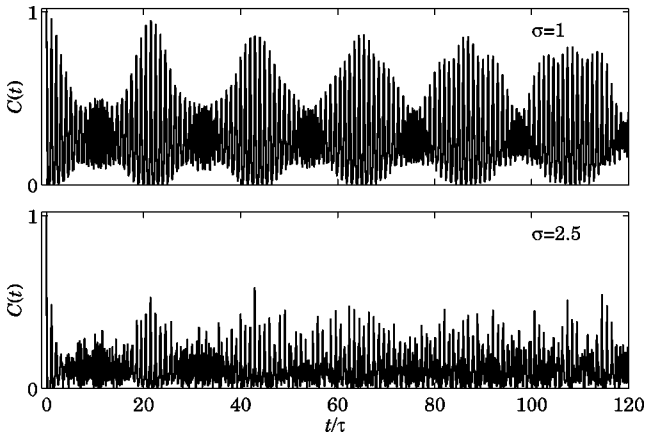

FIG. 3. Autocorrelation function (12) for two circular Gaussian coherent states (9) centered at $n_0=65$ and for two values $\sigma=1$ and $\sigma=2.5$. The initial localization is improved for larger σ; however, collapse times are faster and the revivals are weaker.

$$C(t) = |\langle G(0)|G(t)\rangle|^2. \tag{12}$$

Figure 3 shows the autocorrelation function for two wave packets centered at $n_0=65$ and for $\sigma=1$ and $\sigma=2.5$. Initially, both wave packets are well localized, but the one with $\sigma=2.5$ is more localized. Along the time evolution, if the wave packet is localized, the autocorrelation function is close to 1. The revivals for both wave packets occur at multiples of $t=22\tau$, but the revivals are much stronger for wave packets with smaller $\sigma=1$. Note that the autocorrelation function does not reflect fractional revivals.

IV. FLOQUET STATES OF THE DRIVEN RYDBERG ATOM

The Hamiltonian for the Rydberg atom in a microwave field (2) has as a natural basis the quantum Floquet states [28,29]. The dynamics of the Schrödinger equation for this problem can be reduced to the auxiliary equation (7), a system of time-periodic ordinary differential equations. We can apply standard Floquet theory to the auxiliary equations to calculate a (truncated) basis of Floquet solutions in which any solution of Eq. (7) can be expanded. The Floquet solutions then yield quantum Floquet states for the Hamiltonian (1) using the solution expansion (6) [22].

Let $\Phi(t,0)$ be the matrix of fundamental solutions of the auxiliary equation (7) with $\Phi(0,0)=\mathbb{1}$; that is, any vector solution $a(t)$ with initial conditions $a(0)=a_0$ is obtained as $a(t)=\Phi(t,0)a_0$. The monodromy matrix is defined as $\Phi(T,0)$, where $T=2\pi/\omega$ is the period of the driving field. The eigenvalues σ_n of the monodromy matrix are called the Floquet multipliers; a Floquet quasienergy μ_n is defined by $\sigma_n=e^{-i\mu_n T}$. Note that a quasienergy μ_n is obtained modulo ω; that is, $\mu_n=[-i\ln(\sigma_n)/T]\mathrm{mod}\omega$. It is convenient to define a band of width ω in which the quasienergies are defined, $\mu_n \in [-\omega,0]$.

A Floquet solution is obtained by evolving an eigenvector of the monodromy matrix:

$$a^{\mu_n}(t) = \Phi(t,0)x_n(0),$$

where $x_n(0)$ represents the eigenvector corresponding to the quasienergy μ_n. It can be shown [22,30] that there exists a vector $x_n(t)$ of T-periodic functions such that

$$a^{\mu_n}(t) = e^{-i\mu_n t}x_n(t), \quad x_n(t) = x_n(t+T). \tag{13}$$

Quantum Floquet states are then obtained from the Floquet solutions of the auxiliary equations (13) using the expansion (8):

$$|\psi^{\mu_n}(t)\rangle = \sum_n a_n^{\mu_n}(t)|\phi_n\rangle, \tag{14}$$

where $|\phi_n\rangle$ are the unperturbed states of hydrogen. The quantum Floquet states provide a basis for the periodically driven quantum system in the sense that any time-dependent solution $|\psi(t)\rangle$ of the Hamiltonian (2) can be obtained as a superposition of Floquet states,

$$|\psi(t)\rangle = \sum_n c_n|\psi^{\mu_n}(t)\rangle. \tag{15}$$

The construction of a driven coherent state, as we will define below, requires the computation of a Floquet basis for the auxiliary equations, which are necessarily truncated. A large enough basis set of unperturbed states must be considered so that all interacting states are in the basis and the system does not saturate. The coupling term may cause that many unperturbed states interact. Note that at $t=0$, a Floquet state (14) is a superposition of unperturbed states $|\phi_n\rangle$, with coefficients given by the components of the eigenvectors $x_n(0)$ [see Eqs. (13)]. A Floquet state may be a superposition of many unperturbed states, and its evolution depends on the the Floquet solutions (13). However, at times multiple of the field period $T=2\pi/\omega$, the Floquet states correspond to a phase rotation of the state at $t=0$. Also note that at times $t=kT$, the Floquet states in the velocity gauge (1) and length gauge (1) coincide [see the expansions (6) and (8)].

The direction of the radiation field, the z axis, determine the following selection rules for interacting states:

$$m' = m, \quad l' = l \pm 1. \tag{16}$$

Each quantum number m present in the initial condition defines a subspace of unperturbed states with the same m that participate in the time-dependent solution. If the initial probability distribution involves unperturbed states with one fixed quantum number m, only states with the same m will appear in the expansion of the time-dependent solution in terms of unperturbed states. Therefore, the selection rules (16) impose that individual Floquet states be expanded by unperturbed states with the same m quantum number. We say that a Floquet state *belongs to an m subspace*.

The classical electronic distribution of a Floquet state in an m subspace has axial (cylindrical) symmetry with respect to the z axis. As an example, in Fig. 4(a) the localization of a Floquet state with $m=34$ for $t=0$ is represented. This Floquet state, expressed in terms of unperturbed states (14), is projected mainly on the component $|n=35,l=34,m=34\rangle$; it is the closest Floquet state to the circular state with $n=35$, $m=l=n-1$ in the $m=34$ subspace. The strength and frequency

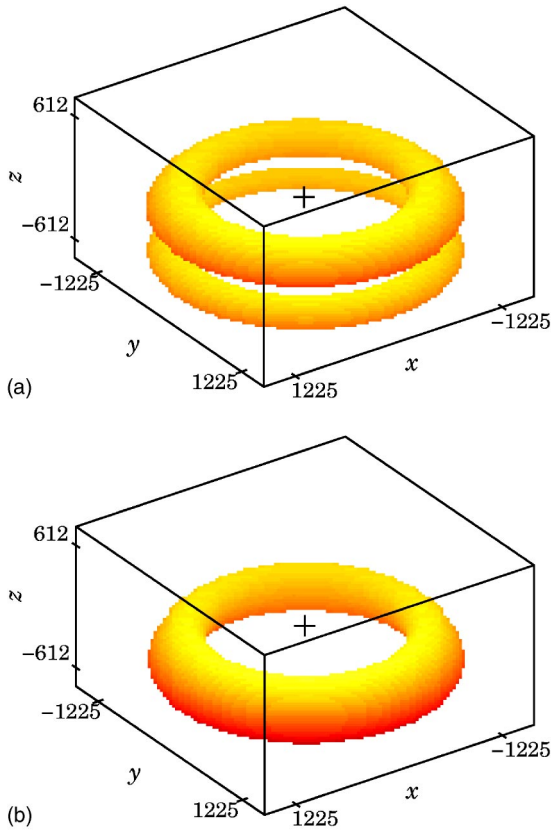

FIG. 4. (Color online) For a microwave field of strength $\lambda = 0.11/n_0^4$, $n_0 = 35$, (a) represents the initial electronic probability distribution of one Floquet state produced with microwave frequency $\omega = 2.5 \times 10^{-5} = 1.094/n_0^3$; this state is not localized in the θ angle. On the other hand, a Floquet state localized in r and θ is shown in (b), produced with field frequency $\omega = 2.6 \times 10^{-5} = 1.15/n_0^3$. These Floquet states are axially symmetric since all interacting states belong to the same m subspace ($m = 34$).

of the driving field used to produce this Floquet states are $\lambda = 0.11/n_0^4$ and $\omega = 1.094/n_0^3$. This Floquet state is localized in r, but it is not localized in the θ angle and, due to symmetry, is of course not localized in the ϕ angle. On the other hand, Fig. 4(b) shows a Floquet state produced with a microwave field of the same strength, but slightly different frequency $\omega = 1.15/n_0^3$. The Floquet states in Fig. 4 have very simple classical space evolution: they oscillate in the z direction at the same rate as the driving field. Note that the choice of driving frequencies for Figs. 4(a) and 4(b) is close to the the classical Kepler frequency $1/n_0^3$; however, the initial electronic distribution can be significantly different. In [18], a *nondispersive* wave packet is constructed with an exact resonance between the classical Kepler frequency and the the driving frequency. However, this condition alone is not enough to obtain a wave packet that is localized, even initially. Tuning of the field strength and frequency is required.

Variation of the parameters λ and ω may have a dramatic effect on the Floquet states. The interaction produced by the microwave field produces an intricate distribution of the Floquet quasienergies within an ω band, in which crossings and avoided crossings occur. In our previous work [22], we study the behavior of the quasienergies as functions of λ or ω. We show that selection rules exist which determine quasienergy crossings and avoided crossings that depend on the multiphoton process involved. We also provide an analytical proof that a quasienergy avoided crossing produces dramatic changes in the Floquet states associated with those quasienergies: the Floquet states are expanded in terms of mainly two unperturbed states [see expression (14)]. This implies that, if such a Floquet state is populated, Rabi-type probability transitions occur.

The localization of the Floquet states is greatly affected by an avoided quasienergy crossing, due to the wide expansion in unperturbed states. This is illustrated in Fig. 5. In Fig. 5(a) we show the Floquet quasienergies as a function of λ for states within the $m = 34$ subspace. The Floquet states associated with the two quasienergies having an avoided crossing are shown in Fig. 5(a) to 5(g). Since their electronic distribution is axially symmetric, only a slice in (x,z) plane is shown ($y = 0$ and positive x). The localization of the Floquet states varies smoothly as a function of the parameter λ; for this figure, three values of λ in the interval where the avoided quasienergy crossing occurs are illustrated. The subplots Figs. 5(b), (c), and (d) correspond to the upper quasienergy in Fig. 5(a), the subplots in Figs. 5(e), (f), and (g) to the lower quasienergy. We note that these two Floquet states virtually exchange their properties during the avoided crossing.

V. DRIVEN GENERALIZED COHERENT STATES

The Hamiltonian for the Rydberg atom in a microwave field in the length gauge (2) is expressed in the extended phase space as the *Floquet Hamiltonian*, given by

$$\mathcal{H} = \frac{p^2}{2} - \frac{1}{r} - z\lambda \cos\theta + \omega I, \tag{17}$$

where (θ, I) is an additional pair of canonical conjugate variables and, quantum mechanically, $I = -i\partial/\partial\theta$.

The Floquet Hamiltonian $\mathcal{H}$ can be diagonalized as

$$\mathcal{H}|\psi_n\rangle = \mu_n|\psi_n\rangle. \tag{18}$$

The eigenvalues μ_n coincide with the Floquet quasienergies [28]. The eigenstates $|\psi_n\rangle$ are the quantum Floquet states $|\psi^{\mu_n}\rangle$, Eq. (14), but they are *stationary* in the extended phase space. This motivates us to construct generalized coherent states for the Floquet Hamiltonian *in the extended phase space*, using the expression for generalized coherent states of conservative systems (9).

We define a Gaussian-generalized coherent state for a periodically driven system as

$$|F, n_0, \varepsilon_0, t\rangle = \sum_{n=0}^{\infty} \frac{\exp\left[-\frac{1}{4}\frac{(n-n_0)^2}{\sigma^2}\right]}{[N(n_0)]^{1/2}} e^{i\mu_n \varepsilon_0} |\psi^{\mu_n}(t)\rangle, \tag{19}$$

where $N(n_0)$ is defined as in Eq. (10); μ_n are the quasienergies, and $|\psi^{\mu_n}\rangle$ are the Floquet states.

A generalized coherent state formed by Floquet states can be constructed if the selected Floquet states satisfy two con-

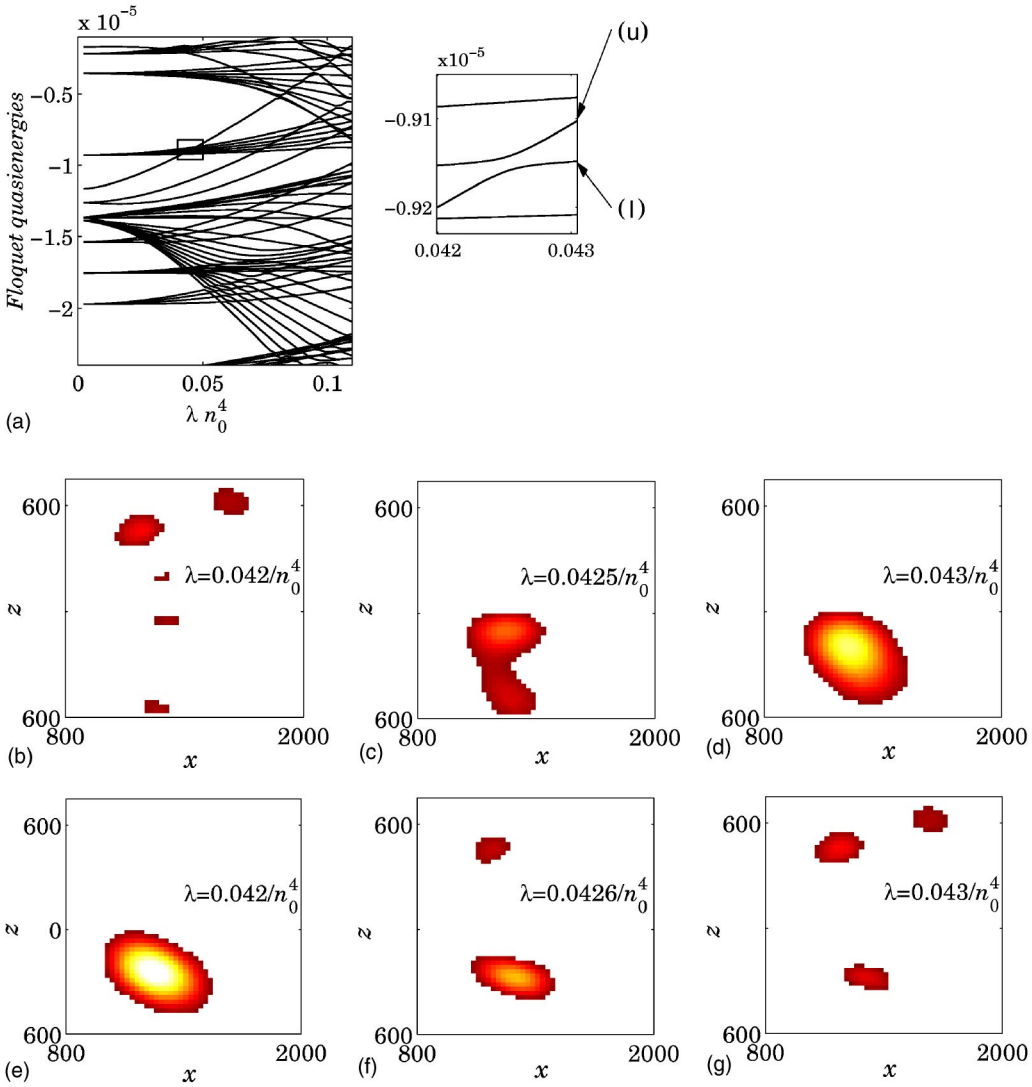

FIG. 5. (Color online) (a) Floquet quasienergies as a function of driving field strength λ, for fixed frequency $\omega=1/n_0^3$, with $n_0=35$. All Floquet states are within the $m=34$ subspace. The zoom-in panel shows two quasienergies featuring an avoided crossing. (b), (c), and (d) Floquet state corresponding to the upper quasienergy having an avoided crossing [marked as "(u)"], for three different values of the field strength λ close to the avoided crossing; the plot represents the probability density in the slice $\varphi=0$. Darker color represents lower probability density, and lighter color is higher probability. (Recall that the Floquet states have axial symmetry with respect to the z axis.) (e), (f), and (g) Floquet state for the lower quasienergy [marked us "(l)"].

ditions. First, each participating Floquet state should be localized in r and θ; this requires that the selected Floquet states correspond to quasienergies that are "far" from avoided quasienergy crossings, which involves a careful tuning of the field parameters λ and ω. The second condition refers to the localization in φ. It was discussed above that the Floquet states are axially symmetric; i.e., their electronic density is evenly distributed in the φ (azimuthal) angle. Therefore, localization in φ can only be achieved by combining Floquet states in different m subspaces. A localized wave packet of the form (19) should include enough Floquet states that belong to different m subspaces.

In Fig. 6, a wave packet formed by a Gaussian distribution of Floquet states and its time evolution is showed. The selection of parameters is $n_0=35$, $\lambda=0.11/n_0^4$, $\omega=1.15/n_0^3$, $\sigma=1.2$, and $\varepsilon_0=0$. The time has been normalized by the period of the driving field, $T=2\pi/\omega$. This wave packet constitutes a coherent state for the driven system, constructed as a Gaussian distribution of Floquet states, one Floquet state for each m subspace. We want to include Floquet states that are close to the circular states $l=m=n-1$, with the main quantum numbers n in a discrete Gaussian distribution centered at $n_0=35$ [see Eq. (19)]. Hence, for each index n, an m subspace was determined by fixing $m=n-1$. In each m subspace, a set of unperturbed states was formed by all the interacting l states within a large range of main quantum numbers n. The time-dependent solution (coherent state) was obtained by solving the auxiliary equation (7) for a large set of unperturbed states that corresponds to the algebraic sum of many m subspaces. The recurrence time of the wave packet in Fig. 6 is not related to the Kepler period τ anymore; nor is it related to the field period T. Although the

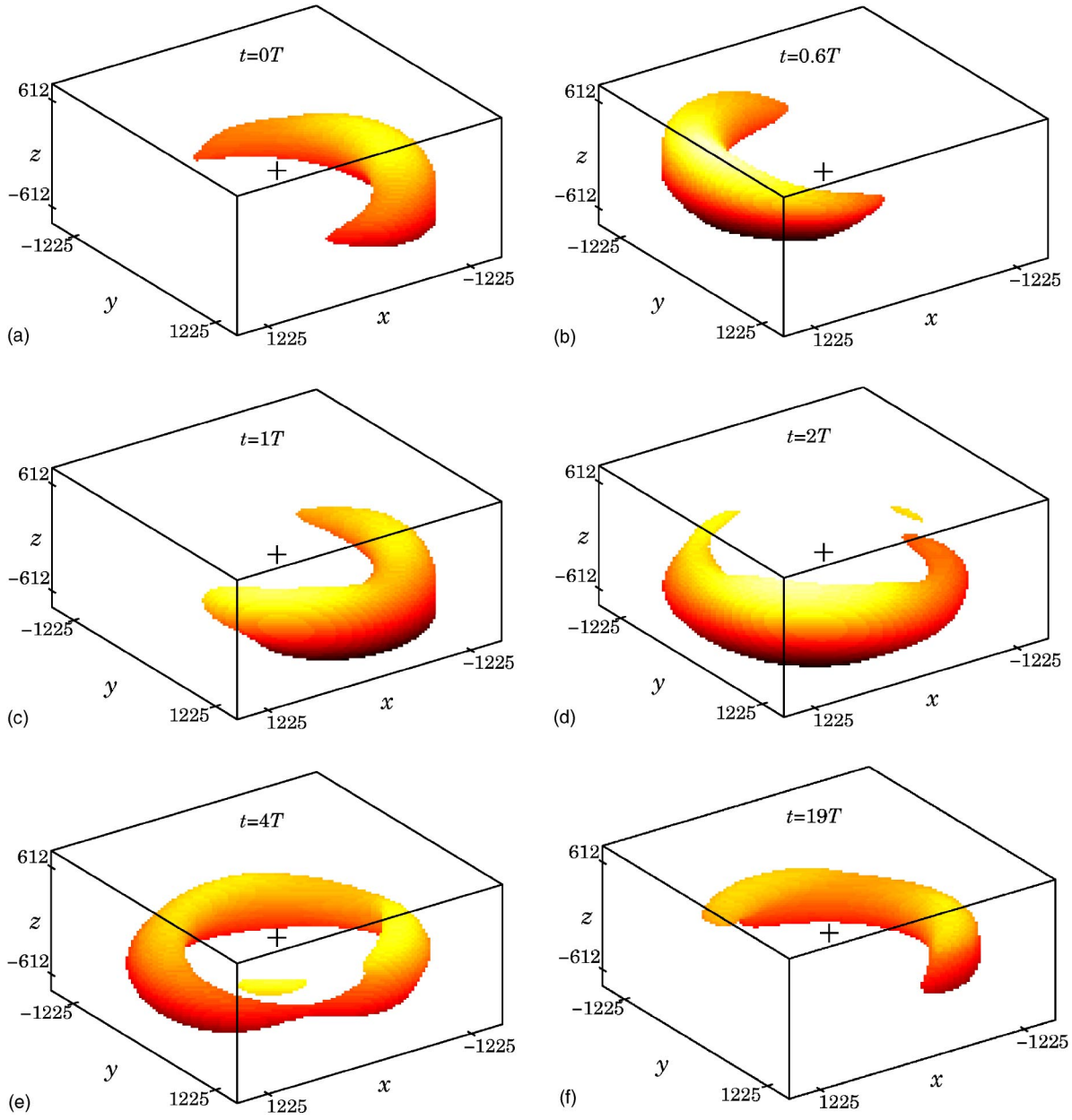

FIG. 6. (Color online) Dynamical evolution of a driven Gaussian coherent state. Microwave parameters $\lambda=0.11/n_0^4$, $\omega=2.6\times10^{-5}=1.15/n_0^3$, and $n_0=35$.

wave packet is centered at a Floquet state which mainly projects to the circular state with $n=n_0=35$, the effect of the microwave field is to include states with higher main quantum numbers n's, increasing the recurrence time. However, the recurrence time is hard to predict analytically, since the components of the Floquet states vary greatly with the parameters λ and ω. The revival time is also very different from the revival time for an unperturbed coherent state, since it is now determined both by the quasienergies participating in the coherent state and by the components of the Floquet states. The coherent state in Fig. 6 has a revival time of about $19T$; in our computations, the wave packet maintained revivals approximately at multiples of $19T$ up to $200T$.

VI. QUANTUM-CLASSICAL CORRESPONDENCE

In general, the construction of coherent states is intrinsically linked to the classical dynamics of Hamiltonian systems. The first coherent states were constructed by Schrödinger as states of the simple harmonic oscillator that were localized in configuration and momentum space, in the sense that they are minimum uncertainty states; they are invariant under the evolution operator, and their expectation values follow exactly the classical orbit. In the following, we provide numerical evidence to show that the coherent state for the driven hydrogen atom constructed in Sec. V has expectation values that evolve according to the classical dynamics. The wave packet of the form (19), represented in

Fig. 6, involves a number of significant quasienergies interacting with the frequency ω of the radiation field. Although in general such construction is expected to disperse in configuration space, we observed in our computations that the wave packet features revivals at an approximately constant revival time of 19 periods of the field. The wave packet shows oscillations in the z direction at exactly the same rate as the microwave field. However, the recurrence time is not related to the external frequency. In the following, we provide a detailed description of the classical dynamics of this system.

The Hamiltonian function for the hydrogen atom in a microwave field (2) is a system of three degrees of freedom with explicit time dependence; the phase space is of dimension 7. The classical equations of motion are given by

$$\dot{x} = p_x, \quad \dot{p}_x = -\frac{x}{r^3},$$

$$\dot{y} = p_y, \quad \dot{p}_y = -\frac{y}{r^3},$$

$$\dot{z} = p_z, \quad \dot{p}_z = -\frac{z}{r^3} + \lambda \cos(\omega t). \tag{20}$$

We want to compare the phase space dynamics of Eqs. (20) with the dynamical evolution of our proposed coherent state (19), as shown in Fig. 6. In all the following, the parameters are fixed as $\omega = 1.15/n_0^3$, $\lambda = 0.11/n_0^4$, and $n_0 = 35$.

The initial conditions for the classical trajectories are chosen close to the expectation values of the wave packet at $t = 0$. For the wave packet in Fig. 6, the expectation values, after rescaling with $n_0 = 35$ according to the transformation (5), are

$$\langle x \rangle \approx -1, \quad \langle p_x \rangle = 0,$$

$$\langle y \rangle = 0, \quad \langle p_y \rangle \approx -1,$$

$$\langle z \rangle \approx -0.18, \quad \langle p_z \rangle = 0.$$

We now proceed to analyze the phase-space structure in the slice defined by the previous expectation values: the plane (x, p_y) with $z = -0.18$, $y = p_x = p_z = 0$, in the region around the point $(x, p_y) = (-1, -1)$.

Wavelet-based time-frequency analysis

A suitable tool to analyze the classical trajectories is time-frequency analysis based on wavelets. The method has been previously used to study high-dimensional systems in molecular dynamics [24] and in celestial mechanics [23]. The main idea of the method is to compute the continuous wavelet transform of the classical trajectories seen as time series or signals. The wavelet transform provides a time-frequency representation of each component of the trajectory, from which the time-varying frequency can be extracted [23,24,31]. Since regular trajectories have frequencies that are constant in time, quasiperiodic and resonant areas in phase space can be determined by calculating the time-varying frequency associated with the initial condition of the trajectory. Chaotic areas are identified with trajectories for which the frequency varies greatly in time.

The wavelet transform of a signal $f(t)$ is defined as

$$Wf(a,b) = \frac{1}{\sqrt{a}} \int f(t) \psi^* \left(\frac{t-b}{a} \right) dt,$$

where ψ is known as the *mother wavelet*. It is defined in terms of two parameters: a is called the scale and it is related to the inverse of the frequency, and b is the time parameter that slides the wavelet to localize the signal. Hence, the wavelet transform can be interpreted as the expansion of the signal in the time-frequency domain. The main advantage of the wavelet transform is that the wavelet adjusts its shape automatically to the frequency in question to obtain better localization of the time series.

The mother wavelet used here is the Morlet-Grossman wavelet, given by $\psi(t) = (1/\sigma\sqrt{2\pi}) e^{2\pi i \lambda t} e^{-t^2/2\sigma^2}$, where σ and λ are parameters that can be tuned to obtain better localization. To illustrate the use of the wavelet transform, consider two trajectories for the system (20). In Fig. 7(a), a regular and a chaotic trajectory are shown, with the configuration variables x, y, and z as a function of time; Fig. 7(b) shows the absolute value of the wavelet transform of these trajectories, as a color-coded function, on the time-frequency plane. The wavelet transform concentrates along a ridge that defines the time-varying frequency. Details of the definition of the instantaneous or time-varying frequency and methods to compute it from the wavelet transform can be found in [23,24,31].

When the time-varying frequency is computed, we have a frequency representation of the trajectory. For a regular trajectory, the time average of the frequency denotes the usual frequency (as defined with Fourier analysis). For a chaotic trajectory, the time average of the instantaneous frequency is not a physical quantity; however, this average varies considerably in reference to neighboring trajectories. A frequency map can be constructed associating the time-averaged frequencies with the initial condition of the trajectory. We computed the frequency map for a mesh of initial conditions in the plane of interest (x, p_y) $(z = -0.18, y = p_x = p_z = 0)$. The frequency map is illustrated in Fig. 8 as a color-coded function on the plane (x, p_y); Fig. 8(a) shows the frequency map for x and Fig. 8(b) the frequency map of z. Although not shown, the frequency map of y is almost identical to the frequency map of x. The regular regions in phase space can be detected as the areas where the averaged frequency varies regularly; on the other hand, the areas where the averaged frequency is irregular correspond to chaotic trajectories. The frequency map of z shows that, at a certain distance from the origin, chaos results from the equal interaction of the Coulomb force with the driving. At further distance from the origin, there is a large region of regular trajectories, which in some areas alternates with chaotic motion. However, all regular trajectories in that zone are characterized by the frequency of z locked with the frequency of the driving field ($\omega = 1.15$). Only the z component of the trajectory locks with the driv-

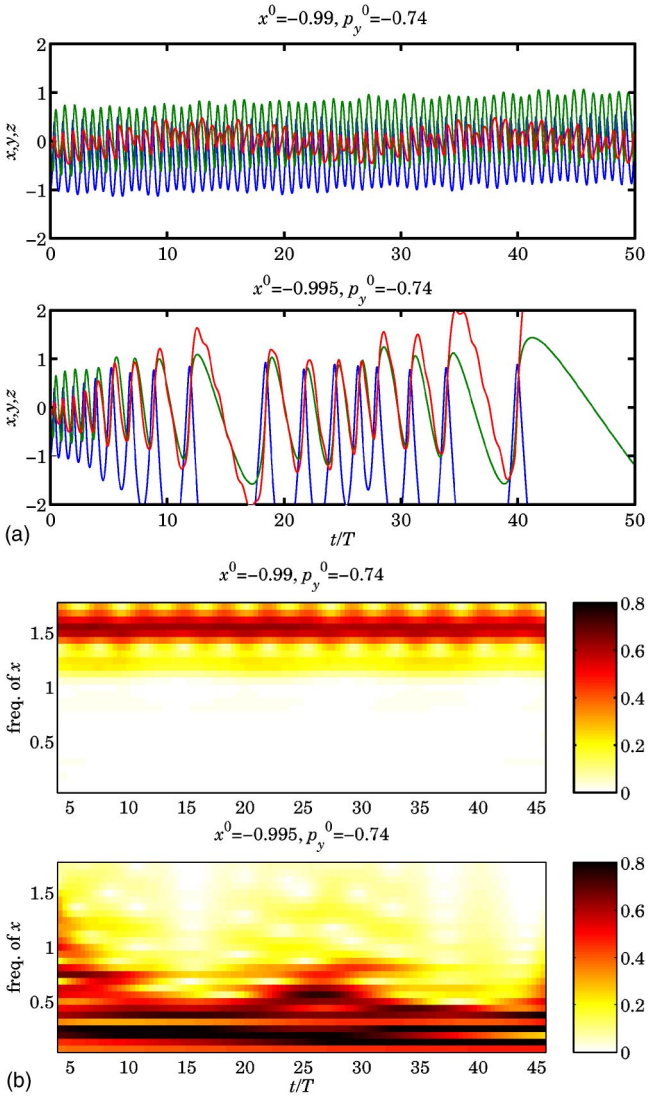

FIG. 7. (Color online) (a) A regular trajectory and a chaotic trajectory in the slice of interest of the phase space: $z=-0.18$, $y=p_x=p_z=0$. $\omega=1.15/n_0^3$, $\lambda=0.11/n_0^4$, and $n_0=35$. In (b), the wavelet transform of each trajectory is shown as a color-coded function of the time-frequency plane.

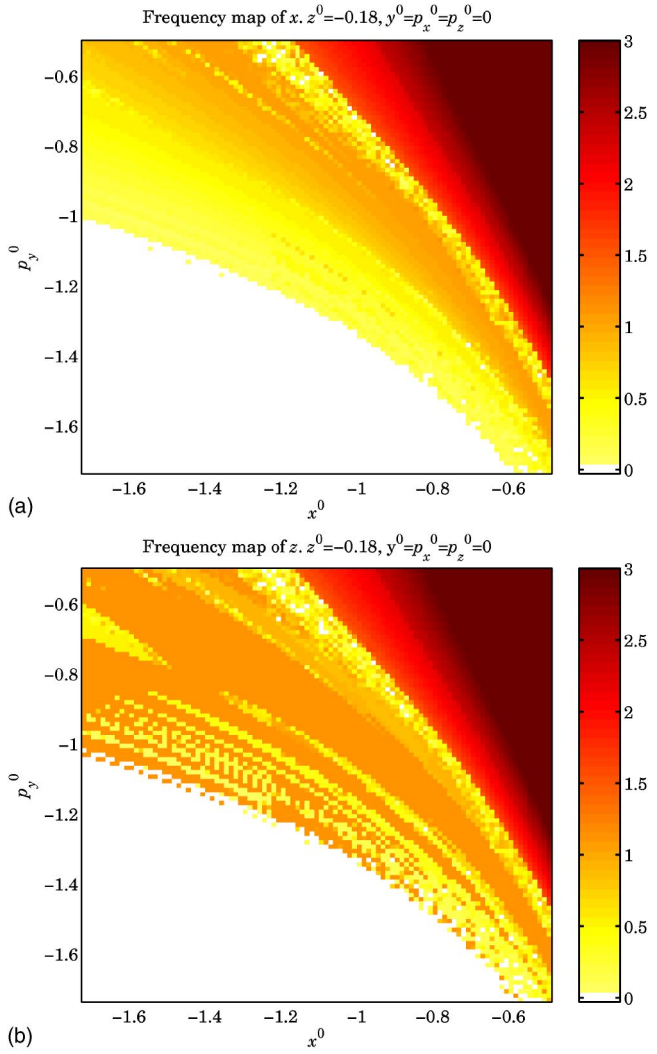

FIG. 8. (Color online) Color-coded averaged frequencies associated with trajectories with initial conditions in the plane (x,p_y).

ing, while the frequency of x and y varies with the distance from the origin. The large regular region with z in resonance with the external frequency can be considered as a higher-dimensional analog of a resonance island usually observed in a (two-dimensional) Poincaré map.

We note, particularly, that the region around $(x^0,p_y^0)=(-1,-1)$ corresponds to regular trajectories. This region corresponds to the expectation values of the driven coherent state shown in Fig. 6, for $t=0$. The classical localization of this wave packet is precisely in the large regular region in which z is in resonance with the external frequency $\omega=1.15$. To compare the dynamics of the classical trajectories with the evolution of the coherent state, we compute the expectation values of the wave packet as a function of time. Such expectation value of x is shown in Fig. 9; whenever the wave packet loses localization, the expectation value is close to zero. In the figure, we also show the classical trajectory with initial conditions given by the expectation values of the wave packet at $t=0$. We can observe that, whenever the wave packet is localized, the expectation value and the trajectory coincide exactly, reaffirming the quantum-classical correspondence of the driven Rydberg atom.

VII. CONCLUSIONS

This work describes the construction and analysis of quantum coherent states for periodically driven systems, specifically the Rydberg atom in a periodic microwave field, based on numerically obtained Floquet states of the system. It is shown that the driven coherent state we propose has expectation values along the classical trajectory, providing proof of the quantum-classical correspondence of the driven system.

The construction of the coherent state is based on the analysis of the Floquet Hamiltonian. Since the Floquet states are stationary in the extended phase space, we can apply the definition of Gaussian-generalized coherent states for unperturbed systems. Such a generalized coherent state was shown

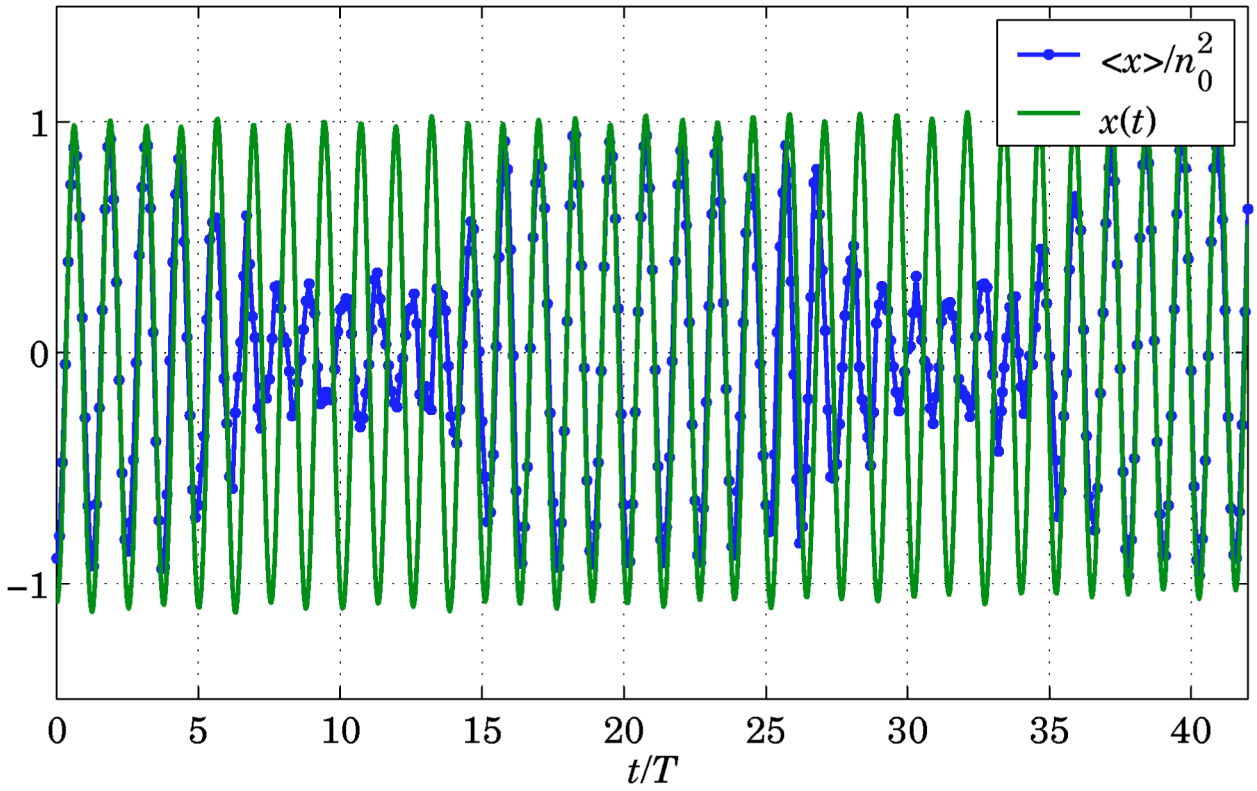

FIG. 9. (Color online) The wave packet of Fig. 6 has expectation values evolving exactly as the classical trajectory. Here we show the evolution of the expectation value $\langle x \rangle(t)$ of the wave packet and the configuration space variable $x(t)$ of the classical trajectory.

to be localized in the configuration space for $t=0$ and have collapses and revivals. However, when compared with the Gaussian-generalized coherent states for unperturbed hydrogen, the recurrence and collapse and revival times are not longer attainable by analytical formulas. The behavior of the driven coherent state is largely more complicated since it depends on the composition of participating Floquet states and their quasienergies, which are obtained numerically.

We analyzed the dramatic effect that the choice of parameters λ and ω, the strength and frequency of the microwave, respectively, have on the phase-space localization of the Floquet states. Avoided crossings of the quasienergies produce delocalization of the Floquet states; hence, the tuning of parameters in order to "avoid" quasienergy avoided crossings is the first step in the construction of the driven coherent state.

We selected Floquet states that are close to circular unperturbed states of hydrogen. The Gaussian superposition of such Floquet states proved to be a localized wave packet, whose dynamics matches exactly the classical dynamics of the system. The wave packet is initially well localized, and as it evolves in time it shows spreading along the classical orbit and revivals. The recurrence and collapse and revival times depend on the quasienergies and components of the Floquet states forming the coherent state.

The wavelet-based time-frequency analysis is an excellent tool to unveil the classical dynamics of the Rydberg atom in a microwave field due to its ability to determine the phase space structure of high-dimensional systems. The Rydberg atom in a microwave field is a Hamiltonian system of three degrees of freedom with explicit time dependence; the phase space is of dimension 7. We detected a large region of the phase space formed by regular trajectories, in which the z coordinate is in resonance with the external field. The driven coherent system we constructed was classically localized in this region. Furthermore, we show that the expectation values of the wave packet follow the classical trajectory.

The driven coherent states constructed as a Gaussian distribution of Floquet states that are close to circular unperturbed states represent a formulation of a wave packet which will remain localized along the classical orbit for a long time. The Floquet states take a very long time to ionize due to small couplings with the continuum [18]; hence, the analysis based on the discrete spectrum of hydrogen remains valid for the calculation of Floquet states and their dynamics.

[1] E. Schrödinger, Naturwiss. **14**, 137 (1926).
[2] R. J. Glauber, Phys. Rev. **131**, 2766 (1963).
[3] W. M. Zhang, D. H. Feng, and R. Gillmore, Rev. Mod. Phys. **62**, 867 (1990).
[4] L. S. Brown, Am. J. Phys. **41**, 525 (1973).
[5] J. Mostowski, Lett. Math. Phys. **2**, 1 (1977).
[6] A. M. Perelomov, Commun. Math. Phys. **26**, 222 (1972).
[7] A. O. Barut, *Dynamical Groups and Generalized Symmetries in Quantum Theory*, 1st ed. (University of Canterbury Press, Christchurch, New Zealand, 1972).
[8] J. A. Yeazell and C. R. Stroud, Phys. Rev. A **35**, 2806 (1987).
[9] J. R. Klauder, J. Phys. A **29**, L293 (1996).
[10] R. F. Fox, Phys. Rev. A **59**, 3241 (1999).
[11] A. ten Wolde, L. D. Noordam, A. Lagendijk, and H. B. Van Linden van Den Heuvell, Phys. Rev. Lett. **61**, 2099 (1988).
[12] J. Parker and C. R. Stroud, Phys. Rev. Lett. **56**, 716 (1986).
[13] G. Alber, H. Ritsch, and P. Zoller, Phys. Rev. A **34**, 1058 (1986).
[14] J. C. Gay, D. Delande, and A. Bommier, Phys. Rev. A **39**, 6587 (1989).
[15] I. Bialynicki-Birula, M. Kalinski, and J. H. Eberly, Phys. Rev. Lett. **73**, 1777 (1994).
[16] A. Buchleitner and D. Delande, Phys. Rev. Lett. **75**, 1487 (1995).
[17] P. Bellomo, C. R. Stroud, D. Farrelly, and T. Uzer, Phys. Rev. A **58**, 3896 (1998).
[18] A. Buchleitner, D. Delande, and J. Zakrzewski, Phys. Rep. **368**, 409 (2002).
[19] H. Maeda and T. F. Gallagher, Phys. Rev. Lett. **92**, 133004 (2004).
[20] H. Maeda, D. V. L. Norum, and T. F. Gallagher, Science **307**, 1757 (2005).
[21] A. Buchleitner and D. Delande, Phys. Rev. Lett. **71**, 3633 (1993).
[22] L. V. Vela-Arevalo and R. F. Fox, Phys. Rev. A **69**, 063409 (2004).
[23] L. V. Vela-Arevalo and J. E. Marsden, Class. Quantum Grav. **21**, S351 (2004).
[24] L. V. Vela-Arevalo and S. Wiggins, Int. J. Bifurcation Chaos Appl. Sci. Eng. **11**, 1359 (2001).
[25] R. F. Fox and M. H. Choi, Phys. Rev. A **64**, 042104 (2001).
[26] M. Nauenberg, Phys. Rev. A **40**, 1133 (1989).
[27] M. Nauenberg, in *Coherent States: Past, present and future*, edited by D. H. Feng, J. R. Klauder, and M. R. Strayer (World Scientific, Singapore, 1994).
[28] J. H. Shirley, Phys. Rev. **138**, B979 (1965).
[29] H. Sambe, Phys. Rev. A **7**, 2203 (1973).
[30] M. Farkas, *Periodic Motions*, 1st ed. (Springer-Verlag, New York, 1994).
[31] L. V. Vela-Arevalo, Ph.D. thesis, California Institute of Technology, 2002.